WATER RESOURCES RESEARCH, VOL. 49, 6381–6392, doi:10.1002/wrcr.20512, 2013

Precipitation predictability associated with tropical moisture exports and circulation patterns for a major flood in France in 1995

Mengqian Lu,[1,2] Upmanu Lall,[1,2] Aurélien Schwartz,[3] and HyunHan Kwon[4]

Received 5 April 2013; revised 28 August 2013; accepted 29 August 2013; published 7 October 2013.

[1] Atmospheric Rivers (ARs) are being increasingly identified as associated with some extreme floods. More generally, such floods may be associated with tropical moisture exports (TMEs) that exhibit relatively robust teleconnections between moisture source regions and flood regions. A large-scale flood event that persisted over Western Europe in January 1995 is studied here. During the last 10 days of the month, two rare flooding events, associated with heaviest rainfall in 150 years, occurred in two places, one over Brittany (West of France), and the second in the France-Germany border region and parts of neighboring countries. In this paper, we explore the month-long evolution of TMEs and their connection to the precipitation events that led to the Brittany event. The persistent large-scale atmospheric circulation patterns that led to the birth, death, and evolution of these TMEs as ARs with landfalls in Western Europe are identified, and the relationship of daily extreme precipitation to these patterns is examined. Singular value decomposition analysis and a generalized linear model are used to assess whether knowledge of the atmospheric circulation patterns from the prior record is useful for explaining the occurrence of their rare events. The analysis establishes the importance of both global and regional atmospheric circulation modes for the occurrence of such persistent events and the hydrologic importance of diagnosing global atmospheric moisture pathways.

Citation: Lu, M., U. Lall, A. Schwartz, and H. Kwon (2013), Precipitation predictability associated with tropical moisture exports and circulation patterns for a major flood in France in 1995, *Water Resour. Res.*, *49*, 6381–6392, doi:10.1002/wrcr.20512.

1. Introduction

[2] Extreme floods have a long history as an important cause of death and destruction worldwide. The recent extreme floods in the United States (1993, 2011), China (1998) [*Zong and Chen*, 2000], United Kingdom (2000 [*Marsh and Dale*, 2002], 2003 [*Marsh*, 2004]), Pakistan (2010) [*Webster et al*., 2011], Europe (1995, 2002 [*Ulbrich et al*., 2003a, 2003b], 2010 [*Bissolli et al*., 2011]), and Thailand (2011) highlight the importance of understanding the hydrometeorological processes responsible for these extreme floods events and the associated temporal and spatial characteristics of sequences of the associated precipitation events. Nonstationarity of flood risk has emerged as an important issue [*Olsen et al*., 1999; *Jain and Lall*, 2000, 2001; *Renard et al*., 2006; *Villarini et al*., 2009; *Katz*, 2010; *Lima and Lall*, 2010; *Massei and Fournier*, 2012] and progress in addressing this concern can only come from an improved understanding of the associated climate dynamics. Various climate change projections [*Trenberth et al*., 2003; *Held and Soden*, 2006; *Allan and Soden*, 2008] suggest an intensification of precipitation in the future, in terms of both frequency and magnitude. The intensity of extreme precipitation is projected to increase under global warming in many parts of the world, even in the regions where mean precipitation may decrease [e.g., *Kharin and Zwiers*, 2000, 2005; *Semenov and Bengtsson*, 2002; *Voss et al*., 2002; *Wilby and Wigley*, 2002; *Wehner*, 2004]. However, these arguments are driven largely by considerations of the moisture holding capacity as a function of temperature, as indicated by the Clausius-Clapeyron (CC) equation [*Muller et al*., 2011; *Romps*, 2011]. Outside the tropics the change in water holding capacity could well be below or above CC scaling whereas in the tropics it has been shown to obey CC scaling [*Muller et al*., 2011; *Romps*, 2011]. We postulate that in the midlatitudes it is important to consider the attendant atmospheric circulation and moisture transport dynamics that lead to persistent extreme precipitation and subsequent flooding as evidenced in the recent major floods cited earlier, and identified as important in Nakamura *et al*.'s [2012] analysis of 21 Ohio River floods that exceed the 10 year return period and in *Lavers et al*.'s [2011a] demonstration of the association between ARs and 10 largest winter floods events since 1970 in Britain. An understanding of the dynamical mechanisms and statistics associated with the frequency and

[1]Department of Earth & Environmental Engineering, Columbia University, New York, USA.
[2]Columbia Water Center, Columbia University, New York, USA.
[3]ENGEES School of Engineering, University of Strasbourg, Strasbourg, France.
[4]Department of Civil Engineering, Chonbuk National University, Jeonju-si, Jeollabuk-do, South Korea.

Corresponding author: M. Lu, Department of Earth & Environmental Engineering, Columbia University, NY, USA. (ml3074@columbia.edu)

0043-1397/13/10.1002/wrcr.20512

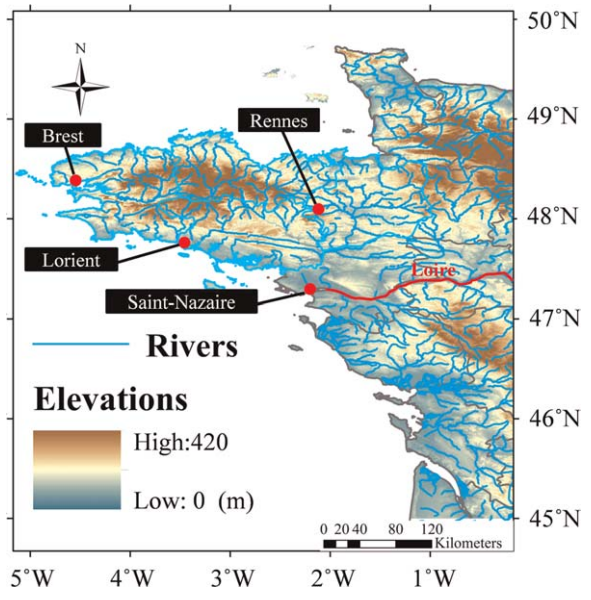

Figure 1. Map of study/inundation area with locations of major cities and flooded river, Loire; Brittany is the area with flood inundation as recorded by the Dartmouth Flood Observatory (http://floodobservatory.colorado.edu/).

structure of such events can aid exploration of their representation in ocean-atmosphere circulation models used for weather prediction, seasonal climate forecasting, and projections of climate change.

[3] Although the climate mechanisms governing precipitation vary by location, several researchers indicate that extreme precipitation events in the midlatitudes are typically associated with anomalous atmospheric moisture from warmer tropical or subtropical oceanic areas. *Bao et al*. [2006] show that enhanced integrated water vapor (IWV) bands, also known atmospheric rivers (ARs) [*Ralph and Dettinger*, 2011], are associated with direct poleward transport of tropical moisture along the IWV bands from the tropics all the way to the extratropics. *Zhu and Newell* [1998] showed that for meridional transport at middle latitudes, ARs account for a substantial part of the moisture transport. There are four or five narrow ribbons across the mid-latitudes, covering <10% of the Earth's circumference, where the majority of the midlatitude moisture fluxes occurred in filamentary features. The AR concept indicated a direction to track the moisture from warmer oceanic source to the heavy precipitated regions. *Schubert et al*. [2011] noted that stationary Rossby waves account for a substantial fraction of summertime monthly mean surface temperature and precipitation variability over a number of regions of the Northern Hemisphere middle latitudes. Further *Knippertz and Wernli* [2010] and *Nakamura et al*. [2012] note that tropical moisture exports (TMEs) to the Northern Hemispheric extratropics are an important feature of the general circulation of the atmosphere and link tropical moisture sources with extratropical precipitation and occasionally with explosive cyclogenesis. *Lavers et al*. [2011a, 2011b] presented evidence that winter flood events in the United Kingdom are connected to ARs, which transport moisture from the subtropical N. Atlantic Ocean to the midlatitudes. The penetration of tropical moisture to the higher latitudes may have considerable impact on extreme precipitation especially poleward of 30°N [*Knippertz and Wernli*, 2010].

[4] Here, we take the 1995 January Flood event in Brittany, Western France, as a case study, and research the following questions:

[5] 1. How was this event related to TMEs or ARs?

[6] 2. What were the moisture sources for this extreme event?

[7] 3. What were the associated atmospheric circulation patterns?

[8] 4. What is the predictability of the 1995 January precipitation using only atmospheric circulation fields identified from the record excluding 1995?

[9] The last question helps identify the importance of different modes of global atmospheric circulation in setting up such a persistent and large-scale event. Thus, the primary goal of the work was to understand the attendant atmospheric circulation and moisture transport dynamics that lead to persistent extreme precipitation and subsequent flooding as evidenced in the 1995 event. Only by understanding how the synoptic atmospheric dynamics regulated the moisture transports and its interaction with local circulation patterns, can we expect to make significant progress in extreme precipitation predictions and floods forecasts.

[10] This paper is organized as follows. Section 2 provides the background of the event used to perform the diagnosis and analysis. Section 3 describes the data used in the study. Section 4 introduces methodology used throughout this paper. Section 5 presents the results and discussions. Finally, section 6 provides a summary and conclusions.

2. Background

[11] The Dartmouth Flood Observatory (DFO, http://floodobservatory.colorado.edu/) recorded two major floods over Western Europe in January 1995. One occurred in Brittany, Western France, from the 20th to the 30th of January. The other was recorded over France, Germany, Netherlands, Belgium, and Luxembourg from the 23rd January to the 7th of February. Although these floods are recorded as two events, they are nearly concurrent, geographically close and associated with a similar persistent rainfall pattern. Hence, from a climate context, these two events are studied as one big event. This was the one of the worst flood events since 1888. It was triggered by heavy persistent rainfall on snow. An estimated 46 people died and 299,100 people were displaced. The heavy rainfall broke the 150-year record in Brittany, and the flood around the Rhine, near Cologne, Germany, was the worst in a century (Dartmouth Flood Observatory Archive, http://floodobservatory.colorado.edu/).

[12] Instead of the whole affected area (France, Germany, Belgium, etc.), we chose the Western France, from 43°N–53°N and 10°W–5°E, as our study region. The heavy precipitation that triggered this flood event started in Western France. This region may better represent the landfall of the AR and may be less influenced by the rain-snow and topographic influences associated with the larger region. The very west of France is composed of numerous small coastal watersheds (Figure 1), which have very low relief. The rivers flow to the Atlantic Ocean or to the English

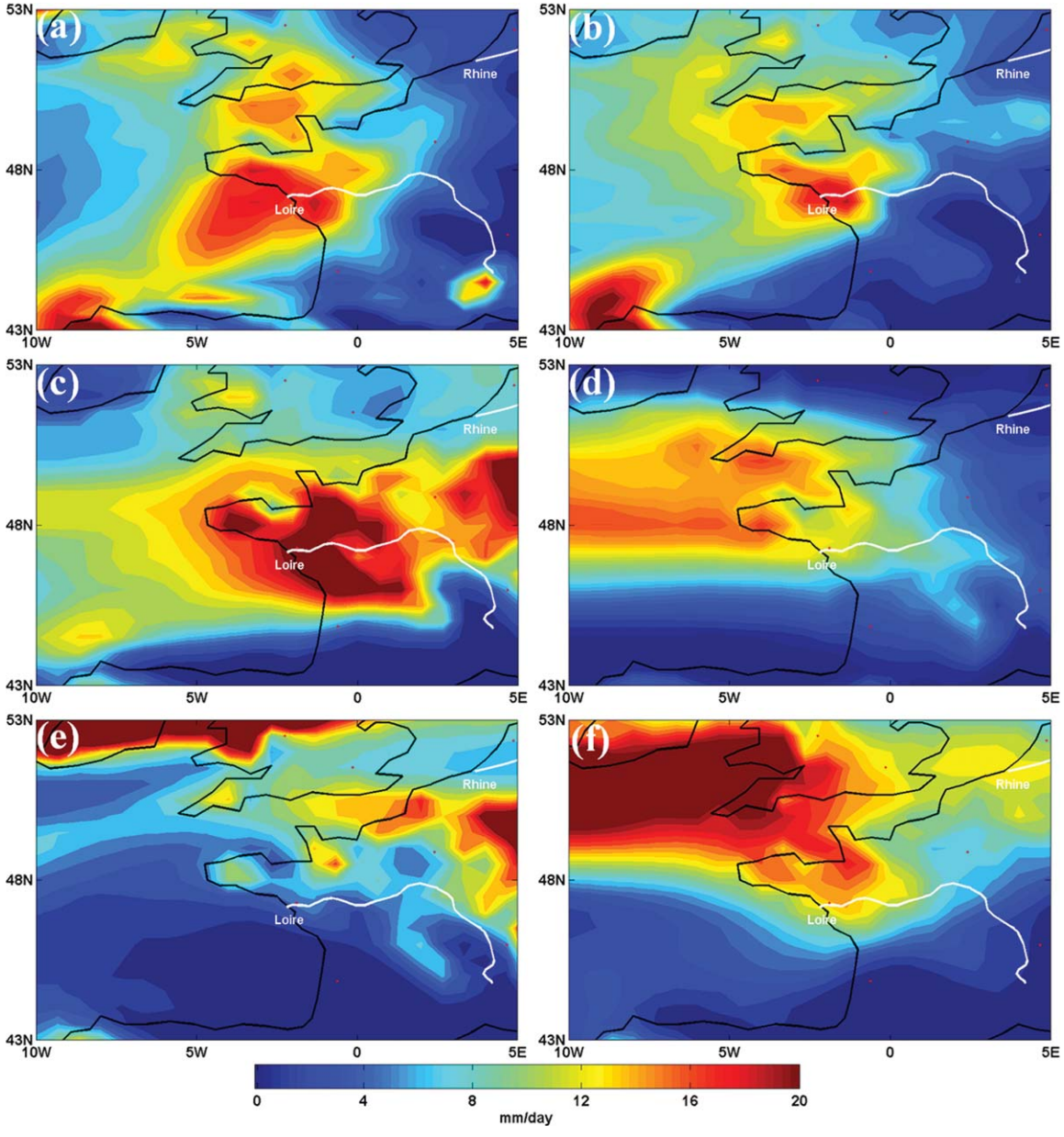

Figure 2. The space-time rainfall patterns in the study area (43°N–53°N, 10°W–5°E) during the heavy rainy days (from left to right, top to bottom): (a) From 9 am on the 17th to 4 am on the 18th; (b) From 6 am on the 19 th to 8 am on the 20th; (c) From 8 am on the 21st to 5 am on the 23rd; (d) From 0 am on the 24th to 0 am on the 25th; (e) From 0 am on the 25th to 0 am on the 26th; (f) From 0 am on the 27th to 0 am on the 28th. The color bar shows the scale; the precipitation flux is in unit mm/day.

Channel (Figure 1). These basins are very sensitive to heavy rain. Brittany (highlighted area in Figure 1), one of these watersheds, typically experiences rainfall from frontal storms coming in from the ocean.

[13] The average rainfall over the last 10 days of the two flood events was twice the climatological monthly average. The area-averaged rainfall of 90 mm within 72 h and daily maximum of 61 mm (National Weather Board of France) were records. Prior to the flooding, there were successive waves of rainfall. Those waves are shown in chronological order, with the data drawn from the Giovanni online data system, developed and maintained by the NASA Goddard Earth Science (GES) Data and Information Services Center (DISC; Figure 2). The red color corresponds to area-averaged rain >20 mm of rain per day, which is recognized as very heavy rain in the local area. The heavy rainfall events began on the 17th and lasted till the 26th of January.

[14] The first and second events (Figures 2a and 2b) were both over the upper stream of Loire River (Figure 1), which enters the English Channel, and were responsible for a rise in the river. The third event occurred in the city of Rennes (Figure 1), located in the red zone, with rainfall exceeding its last 50 years daily rainfall record over a two-day continuous rain period from the 21st to the 23rd (Figure 2c). More than 40 mm rain fell during over these two days, breaking almost all the local records. The last three

rainfall events occurred on the 24th (Figure 2d), 25th (Figure 2e), and 27th (Figure 2f), respectively. Although the rainfall magnitudes of the three events were smaller than those of the previous ones, they resulted in a continuous supply of water to the flooded area.

3. Data

[15] In order to track the moisture source and path, we use the TMEs identification technique, introduced by *Knippertz and Wernli* [2010] and later used by *Knippertz et al*. [2012] to produce a global TME climatology. Different meteorological parameters are tracked along the trajectories. The TME dataset organizes the tracks by their birth dates. In this paper, the specific humidity and pressure are used. The moisture source of each trajectory was calculated for every 100 km × 100 km box between 0° and 20°N, and for every 30 hPa between 1000 and 490 hPa. Since the upper bound of the starting region for the trajectories was set to 490 hPa, about 90% of all water vapor is included. Each trajectory represents 3×10^{12} kg of atmospheric mass. Only trajectories that cross 20°N, and reach 35°N within the next 5 to 6 days were retained to ensure that the characteristics of the tropical air parcels are maintained on their way across the subtropics, although changes due to fluxes of heat and moisture from the underlying surface or mixing cannot be completely excluded. Finally, moisture transport trajectories are retained only if their water vapor flux reaches 100 g kg^{-1} m s^{-1} somewhere north of 35°N. Such a flux criterion selects for "fast" events, but tests with a mixing ratio criterion instead showed rather similar results. While the geographical distribution is generally quite robust, the number of trajectories varies with the chosen threshold. The value of 100 g kg^{-1} m s^{-1}was set in order to get robust, yet meaningful statistics [*Knippertz and Wernli*, 2010].

[16] The major climate data source used is Modern Era Retrospective-analysis for Research and Applications (MERRA), which provides a resolution of 1/2° latitude × 2/3° longitude. In this study, we use the daily sea level pressure (SLP) and daily precipitation (P) from MERRA. We use the daily SLP anomaly for the atmospheric circulation pattern analysis. The SLPa is calculated against calendar day climatology of January from 1979 to 2011,

$$SLPa_{ij} = SLP_{ij} - SLPc_i \tag{1}$$

$$SLPc_i = \frac{\sum_{j=1979}^{2011} SLPc_{ij}}{33} \tag{2}$$

where i is the ith day in January; SLPa_{ij} is the SLP anomaly (SLPa) on the ith day in January in year j ($j = 1979$, 1980 … 2011); SLPc_i is the daily climatology of SLP on the ith day of January, or average calendar day SLP.

[17] The daily North Atlantic Oscillation Index (NAO index) is obtained from Climate Prediction Center, NOAA (http://www.cpc.ncep.noaa.gov/products/precip/CWlink/pna/nao_index.html). The daily NAO index is constructed by projecting the daily 500 mb height anomalies over the North Hemisphere onto the loading pattern of the NAO. The loading pattern of the NAO is defined as the first leading mode of Rotated Empirical Orthogonal Function (EOF) analysis of monthly mean 500 mb height during the 1950–2000 period.

4. Methods

[18] In line with the research questions listed earlier, we first use the TME data to assess whether persistent large-scale, organized moisture transport, and convergence over the region was responsible for the flood, and if so, what are the associated moisture sources. Second, we explore what large-scale atmospheric circulation patterns persisted during the event. Instead of focusing on local atmospheric fields or circulation types, we explore the hemispheric circulation fields to gain insights on the scales of organization that may be associated with the event and the large-scale moisture transport. The leading EOFs of January hemispheric SLP fields are used to develop insights into the 1995 circulation and precipitation anomaly. To assess whether the large-scale circulation fields contribute significantly to the event, we build a regression model for area-averaged daily precipitation in the French region of interest with the EOFs of the daily January hemispheric fields as predictors for all years excluding 1995. This model is then used to predict the daily rainfall in January 1995 to establish the extent to which the TME steering by the large-scale circulation can by itself explain the anomalous precipitation in the region. The relative contribution of different spatial scales of the large-scale circulation modes is of interest in developing this predictive model, to help understand how the TME is steered to the area. The model developed is not intended to be a rainfall forecast model.

[19] The first step was to identify the moisture sources for the precipitation associated with the 1995 events. The moisture sources were identified by using a TME dataset to track the moisture transport pathway. First, the global TME data [*Knippertz and Wernli*, 2010] were processed to identify moisture sources and tracks that end with precipitation in our study area for the period of record. Next, a singular value decomposition (SVD) of the SLPa fields for January using the MERRA from NASA GES DISC [*Rienecker et al*., 2011] from 1979 to 2011 was conducted to identify the dominant daily atmospheric circulation patterns. A link to the dominant mode of winter climate variability, the NAO, was also explored. Finally, a generalized linear model (GLM) was used to assess the predictability of rainfall for the 1995 event given the atmospheric circulation patterns identified from the other years.

4.1. TME Birth Analysis and Tracking

[20] Q1: How is the 1995 flood event related to TMEs, associated with midlatitude ARs to the region of interest in France?

[21] Q2: What are the moisture sources for the extreme rain events in the region?

[22] The TME "tracks" database was filtered to retain all the tracks that entered the study area (43°N–53°N, 10°W–5°E) before they died. The TME tracks are available for 7 days from the origin, sufficient to cover the travel time to the region of interest. The TME birth time period of interest is from the 11th to the 19th of January 1995, based on the facts that (1) the heavy precipitation period that

triggered floods was from the 17th to the 26th Jan.; (2) it takes 6 ± 1 days for the tropical moisture to reach the area, depending on the wind speed, and the trajectories of the tracks. Only the moisture tracks that entered the study area 1 or 2 days before the start and end of the heavy precipitated period were selected for further investigation on the changes of specific humidity with time as they propagated from the moisture sources to the study area.

[23] The change of moisture is calculated as $\Delta Q = Q_t - Q_{t+1}$ (1), where t is the time point on the trajectory and $Q_t$is the specific humidity in g/kg (units). There are a total of 29 time points for each of the tracks, sampled every 6 h. Therefore, t ranges from 0 to 28, corresponding to the birth location and the one point before death location. The changes of moisture along the trajectories of the tracks relate to the moisture release and recharge process.

[24] The total release of water from the air parcel, that is, the precipitation, after it entered the study area was quantified by calculating the total difference of total specific humidity (including liquid phase) integrated all the tracks over for a given birth date as follows:

$$\Delta Q^i = \sum_{k=1}^{N_i} \left(Q_k^i(t_{enter}) - Q_k^i(t_{exit}) \right) \tag{3}$$

where i is the birth date index (e.g., $i = 11\text{th}, \ldots, 19\text{th}$), N_i is the number of tracks born on day i, t_{enter} and $t_{exit}$are the time of entering and exiting the study area, respectively.

[25] By interpreting the selected tracks together with the changes of specific humidity, we are able to identify the birth location and their trajectories to the study region and compute the release of water vapor from the moist air parcel, for each birth date, and corresponding source location.

4.2. SVD Analysis of SLPa

[26] Q3: What are the large-scale atmospheric circulation patterns that may be associated with the moisture transport to the study area in January?

[27] Q4: How are the atmospheric circulation patterns identified related to the 1995 extreme rainfall event in the Western French region of interest?

[28] With the aim of understanding the leading modes of daily atmospheric circulation patterns that are active in the midlatitudes and their relation to extreme rainfall events in the study region, a SVD analysis of the SLPa field was used. The SVD has been widely adopted in the atmospheric sciences since its first introduction by *Edward Lorenz* [1956]. This analysis technique enables a description of a multidimensional meteorological field with a relatively small number of spatial patterns that, together, explain a large fraction of the total variability of the field. SVD was first applied in the meteorological context by [*Prohaska*, 1976] to document the simultaneous relationships between monthly mean surface air temperature over the United States and hemispheric SLP patterns. It has been used by [*Lanzante*, 1984] to study the relationship between seasonal mean extratropical SST and 700-mb height anomalies. *Bretherton et al*. [1992] contributed to further popularization of SVD method of detecting temporally synchronous spatial patterns. The SVD method is equivalent to Principle Components Analysis (PCA) [*Sánchez*, 1982; *Gnanadesikan*, 1997; *Everitt and Dunn*, 2001; *Sirca and Horvat*, 2012]. *Cherry* [1997] provides a useful discussion of the application of SVD and PCA and their interpretation with climate data. For a single spatial field with each column standardized (column mean subtracted and then dividing by the column standard deviation), the SVD is simply a numerically stable way of conducting the PCA on a correlation matrix, especially for the case where the number of columns exceeds the number of rows.

[29] SVD was used to analyze the spatial patterns of the daily SLP anomalies defined using the daily calendar day climatology over the period of record, in the midlatitude band (40°N–60°N 180°W–180°E) covering the flooded region. Sometimes, daily fields are prefiltered to form 5 day or 10 day averages before SVD is applied. Here, we are interested in daily extremes and variations in circulation that may relate to both the stationary aspects of atmospheric flow and the transient eddies that transport moisture from the tropic to the midlatitudes. Consequently, we apply the SVD decomposition directly to the daily SLPa data.

[30] We then investigate the association between average daily precipitation for the flooded region (43°N–53°N 10°W–5°E) and the leading EOFs of the midlatitude SLP anomalies. The SLPa data are standardized before the SVD analysis by first subtracting the average calendar day SLP for the grid box over 1979 to 2011, then divided by the corresponding standard deviation.

[31] The SVD analysis applied is as follows. The daily SLP anomaly field for the selected middle latitude band contains a total of $D = d_1 \times d_2$ data points, where d_1 and d_2 are the number of grid cells by latitude and longitude, respectively. Since the MERRA data have a spatial resolution of 1/2° latitude × 2/3° longitude, the midlatitude longitudinal band covers 40°N–60°N, 180°W–180°E, d_1, d_2, and D are 41, 541, and 22,181, respectively. Then let X be a N X D data matrix, where N is the total number of days in January from 1979 to 2011, so $N = 1023$. The SVD of X is a factorization of the form:

$$X = USV^T \tag{4}$$

where $U^TU = I, V^TV = I$ the columns of U are orthonormal eigenvectors of XX^T, the columns of V are orthonormal eigenvectors of dimensions of X^TX, and S is a diagonal matrix containing the square roots of eigenvalues from U or V in descending order, and the dimensions of U, S, V^T are $N \times N$, $N \times D$, and $D \times D$, respectively. The analysis partitions a field into orthogonal (independent) modes. The eigenvalues provide a measure of the variance explained by each mode. The temporal and spatial variabilities of the field are isolated and represented by the columns of U and V, respectively.

4.3. Precipitation Predictability Using EOFs of Hemispheric SLPa Using GLM

[32] Q4: What is the predictability of the 1995 January precipitation using the atmospheric circulation patterns identified from the January data for all years excluding 1995?

[33] The first 20 EOFs derived from the previous analysis are used as candidate predictors of rainfall using a GLM. The area-averaged precipitation in the study region

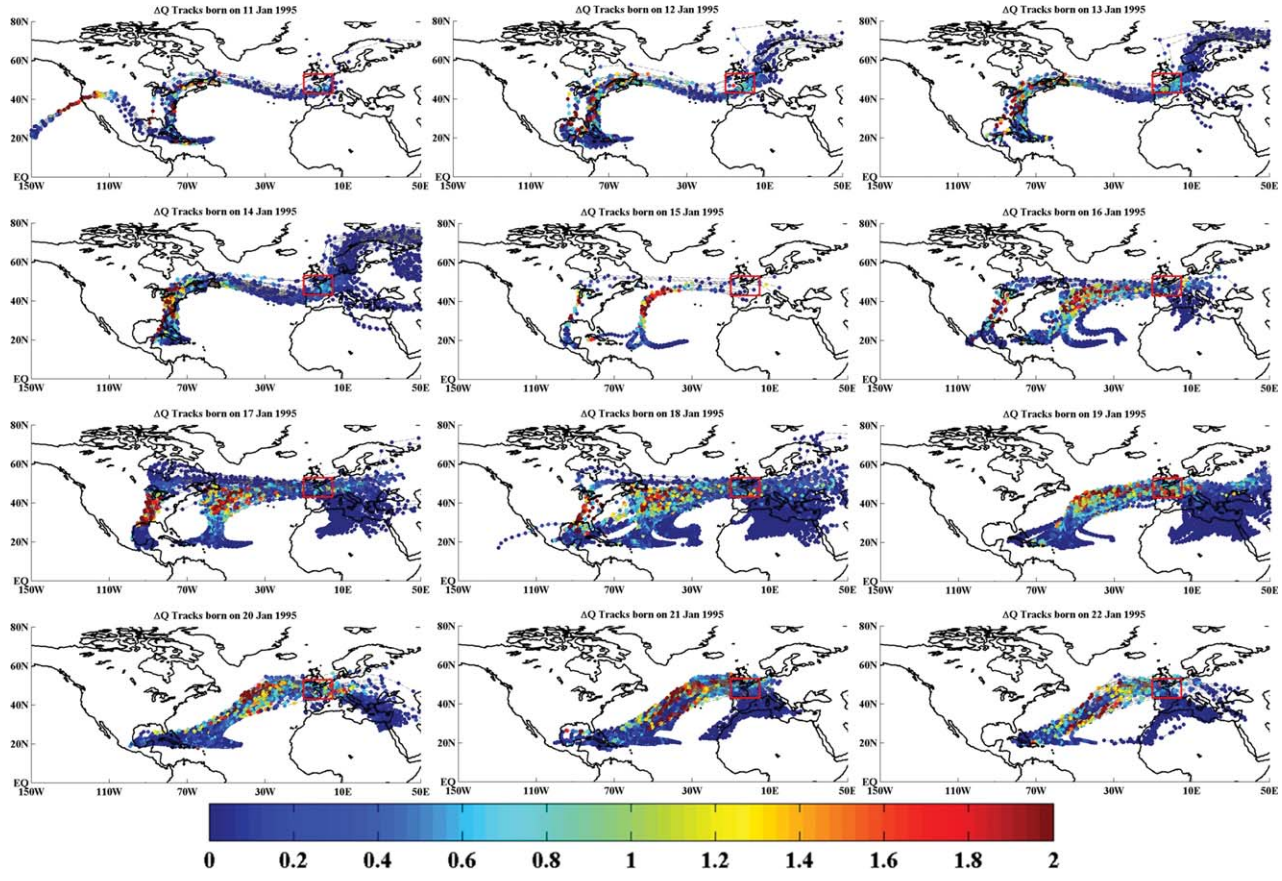

Figure 3. TME tracks born on the 11th to the 22nd of January (from left to right, then from top to bottom), colors depicting moisture release from the air parcel in the study area during heavy rainfall period from the 17th to the 28th of January in 1995. The red box highlights the flooded area. The color bar indicates the specific humidity change (g/kg).

was computed using the MERRA dataset. First, the linear dependence, that is, Pearson correlation between each of the EOFs and the area-averaged precipitation in the study region is computed as

$$\rho_{X,Y} = \frac{E[(X-\mu_X)(Y-\mu_Y)]}{\sigma_X \sigma_Y} \tag{5}$$

where X is one of the EOFs, Y is area-averaged daily precipitation; σ_X and σ_Y are the standard deviations of X and Y, respectively.

[34] The GLM model was fitted in a cross validation mode and tested for 1995 (i.e., using all the data excluding 1995, and predict 1995's area-averaged rainfall using the 1995 SLPa EOFs) to assess rainfall predictability using the atmospheric circulation patterns identified.

[35] The aims of this model are (1) to identify the association of daily rainfall in January with daily circulation modes for the day of rain; (2) test the capability of the model for predicting the area-averaged precipitation over the Western France (red box in Figure 3) for January 1995 without using that data for model fitting; and (3) hence, assess the spatial scales of the atmospheric circulation fields that are most important for predicting January daily rainfall, and their performance for the extreme case in January 1995. We used the time series of selected EOFs from 1979 to 2011 excluding 1995 and area-averaged precipitation over Western France (red box in Figure 3) in all January from 1979 to 2011 excluding 1995. The model is fit by using a R package "*bestglm*" developed by *Mcleod and Xu* [2010] with an extended Bayesian information criterion (BICq). The BIC is a criterion for model selection among a finite set of models. The BIC is closely related to Akaike information criterion with additional penalty term for number of parameters in the model to resolve the problem of overfitting. The BIC was first developed by *Schwarz* [1978]. The BICq is derived by assuming a Bernouilli prior for parameters. Each parameter has a prior probability of q of being included, where $q \in [0, 1]$, and the resulting $\mathrm{BIC_q}$ is defined as

$$BIC_q = D + k\log(n) - 2k\log q/(1-q) \tag{6}$$

When $q = 0$, the penalty is taken to be $-\infty$; therefore, no parameters are selected. And for $q = 1$, the full model with all covariates is selected. Here, we use the default value $q = 0.25$ [*Mcleod and Xu*, 2010] to fit the model, to select a relatively parsimonious set of predictors.

[36] Let $Y = (y_1, y_2, y_3, \ldots, y_n)^T$ be the $n \times 1$ vector of area-averaged rainfall values and $X = (X_1, X_2, X_3, \ldots, X_n)^T$ be the $n \times p$ matrix of the daily concurrent predictor EOFs.

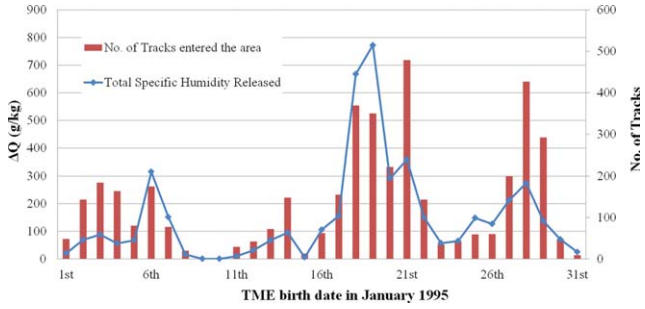

Figure 4. The number of tracks entering the study area from the moisture sources identified as a function of date of birth and the associated release of water. ΔQ is in g/kg.

We assume that the marginal density of Y is a Gamma distribution: $Y = \text{Gamma}(\nu, \lambda)$ with

$$f_Y(y) = \frac{\lambda}{\Gamma(\nu)}(\lambda y)^{\nu-1}e^{-\lambda y}y \geq 0 \tag{7}$$

$$E(Y) = \nu/\lambda = \mu \tag{8}$$

$$\text{Var}\ (Y) = \nu/\lambda^2 = \mu^2/\nu \tag{9}$$

$$\ln(\mu) = \mathrm{X}\boldsymbol{\beta} \tag{10}$$

where $\boldsymbol{\beta}$ is the vector of fitted coefficients.

[37] The performances of both the fitted model and the predictions for the 1995 event are assessed through the variance explained, which are defined as

$$\mathrm{R}^2 = \frac{\text{SStotal} - \text{SSresid}}{\text{SStotal}} \tag{11}$$

$$\text{SStotal} = \sum_{\mathrm{i}} (\mathrm{y_i} - \overline{\mathrm{y}})^2 \tag{12}$$

$$\text{SSresid} = \sum_{\mathrm{i}} (\mathrm{y_i} - \mathrm{f_i})^2 \tag{13}$$

where y_i, $\overline{y}$, and f_i are the ith observation, the average of all the observations, and the fitted value from the aforementioned regression equation. For the fitted model, R^2 provides a measure of the goodness-of-fit with $\mathrm{f_i}$ being the fitted values, while for the prediction of 1995 January event, R^2 indicates the predictability of rainfall using the fitted model.

[38] The importance of each predictor (i.e., EOF in this paper) is evaluated by the change of deviance after eliminating that predictor from the fitted model. Deviance is a measure of the fit for GLM, which in our context is identical to the likelihood ration statistic [*McCullagh and Nelder*, 1989] and is defined as

$$Deviance = -2 \times \left(LL(\beta; y) - LL_{perfect}(\beta^p; y)\right) \tag{14}$$

$$LL(\beta; y) = \log\left(p(y|\beta)\right) \tag{15}$$

$$LL_{perfect}(\beta^p; y) = \log\left(p(y|\beta^p)\right) \tag{16}$$

where $LL(\beta; y)$ and $LL_{perfect}(\beta^p; y)$ correspond to log-likelihood of the a candidate GLM and the perfect GLM,

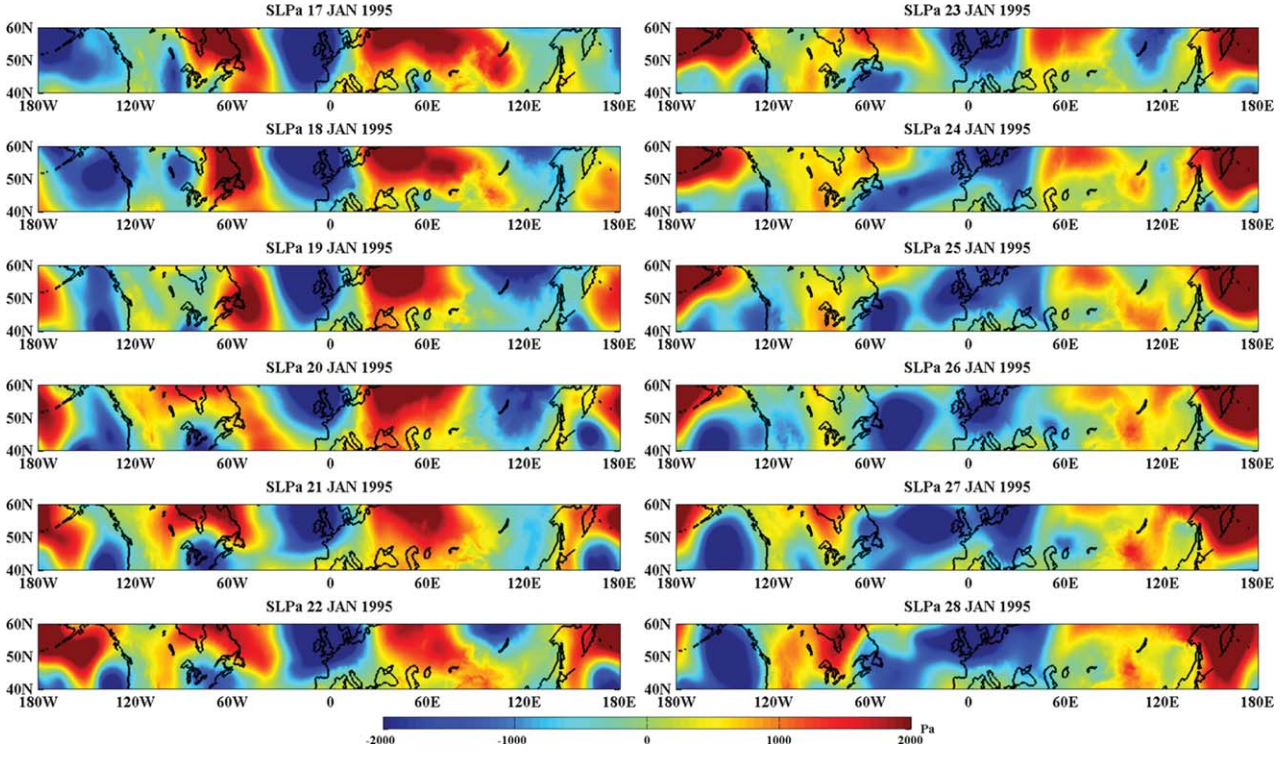

Figure 5. The evolution of the SLPa fields over the precipitation period and the flooding period. The figures display the raw patterns using MERRA data.

Table 1. Correlation Coefficients[a] Between Selected EOFs and Area-Averaged Precipitation Over Study Area[b]

$Cor(i\text{th}\,EOF_t, Precip_t)$					
EOF1	**EOF2**	**EOF3**	**EOF4**	**EOF5**	**EOF8**
0.45	−0.45	0.14	0.11	−0.12	−0.12
EOF10	**EOF12**	**EOF13**	**EOF15**	**EOF16**	
−0.14	0.19	−0.10	0.10	0.11	

[a]All the correlations are statistically significant at $p < 0.05$, against a null hypothesis of no-effect.
[b]Western France, red box in Figure 3.

that is, one where there is an exact prediction of each observation. The β refers to the parameter vector for the model of interest, and β^p to the parameter vector for the perfect model. The difference of deviance between two models measures the significance of the removed predictor, and the statistical significance of the difference can be tested using the χ^2 distribution with 1 degree of freedom.

5. Results and Discussions

5.1. TME Birth Analysis and Tracking

[39] The results of the TME birth analysis and tracking are provided in Figure 3, with colors indicating the changes of specific humidity along the tracks. The key observations are as follows:

[40] 1. There were two major sources of moisture from the tropical oceans, one centered at 20°N, 60°W, around the subtropical region of the North Atlantic, east of the Bahamas, and the other centered at 20°N, 100°W, which reflects the moisture from the Yucatan Peninsula across the Gulf of Mexico. Both regions were also recognized as ones of prominent TME activity maxima in the Atlantic sector in [*Knippertz and Wernli*, 2010].

[41] 2. Despite the fact that the air parcels release water on their way to the study area, there was a considerable amount of water released in the study region from the moist air parcels that originated from the tropics.

[42] The number of tracks that enter and release a large amount of water in the region increases for the birth period from the 11th and remains very large until the 22nd of January. This period corresponds to the heavy rainy days from the 17th to 28th. The total number of tracks that entered the area, contributing to the total precipitation by releasing water vapor they carried from warmer oceanic areas, increased as the dates approach the heavy precipitation period. The total water released from the tracks in the study area also increased, leading to both an increased number of tracks and higher water release from individual air parcels (Figure 4). There is a break of water release with TMEs born on the 15th (that entered the area on the 20th), which is consistent with break of heavy rain on the 20th, and is right before the onset of the worst precipitation wave on the 21st Jan. The water released for the tracks born on the 16th, together with the abrupt jump in the total release of air parcels born on the 18th, contributed to the worst rainfall events during the 21st to the 23rd. The number of tracks entered peaks on the 27th from the tracks born on the 21st. However, the associated water release from the tracks is not as large. This is consistent with reduced rainfall on the 27th. The 6 ± 1 days lag between the generation and arrival of the tracks appear to be a consistent feature that bears further investigation in terms of both the potential genesis of convection in the source regions and the persistence of the large-scale atmospheric circulation patterns associated with the track steering mechanism to the study area.

5.2. SVD Analysis of SLPa and the Predictability of Daily Rainfall

[43] To provide a context for the analysis, the evolution of the SLP anomaly fields over the 1995 precipitation period is shown in Figure 5. The low pressure anomalies over France were well developed since the onset of rainfall on the 17th of January. The low pressure system was persistent during the heavy rainy period from the 17th to the 26th, and started to dissipate and moved northeastward. The sandwich pattern of the two high pressure centers and a trapped low in the middle persisted over the Western France region for almost 7 days, from the 17th to the 23rd, before the breaking of the highs and northeastward movement and dissipation of the low. The trajectory of the low pressure system coincides with the precipitation patterns in Figures 1d–1f: starting from the 25th to the 28th, the path of the rain was turning anticlockwise toward a direction off the west coast of France and rain fell in the English Channel.

[44] The EOF's identified from the SVD analysis of the January 40°N–60°N SLPa fields represent both spatial patterns and corresponding amplitude time series of the EOFs of the space-time gridded SLPa fields. The pattern associated with each EOF also explains a certain fraction of the variance of the 40°N–60°N SLPa field. The EOF's are arranged in order of descending variance explained. The first six (twenty) EOFs explain 53.5% (86.5%) of the total variability in the daily SLPa over 40°N–60°N latitudes and 180°W–180°E longitudes. The EOFs that have a statistically significant correlation with daily precipitation at the 95% significance level are identified in Table 1. The EOFs that are retained using the BIC_q criteria in the GLM model fit for predicting daily precipitation, not using the 1995 data are identified in Table 2. The correlations and the regression coefficients for EOFs 1 and 2 are the largest and are opposite in sign. Their importance is also reflected in the model deviance scores reported in Table 2. The deviance associated with the fitted GLM model is 486 (benchmark). The importance of each predictor is assessed by dropping that predictor from the model and computing the resulting deviance. Large increases in deviance (e.g., 656 from 486 when EOF1 is dropped from the set selected) suggest a high importance of the predictor. The most important predictors (in order) of daily precipitation excluding the 1995 data are then EOFs 1, 2, 8, 12, 13, 4, and 5. All the deviance scores presented in Table 2 for the reduced models are different from what would be expected by chance at the 10% significance level. The difference for EOF5 is significant at the 0.0002 level. The time series for the leading predictors for the 1995 January are presented in Figure 6, to help visualize the role the associated spatial modes of atmospheric circulation may have played in the extreme rainfall events. The space-time patterns of these leading predictors are discussed below.

[45] The spatial patterns associated with selected EOFs (the first six, and then three others that are subsequently

Table 2. Summary of Predictors Selected in the GLM Model

Predictors	Coefficients	p	Deviance with term dropped (the "best" fitted GLM model Deviance = 486)
(Intercept)	−10.69	<0.001	
EOF1	13.30	<0.001	**656**
EOF2	−11.74	<0.001	**613**
EOF3	2.09	<0.001	489
EOF4	4.11	<0.001	504
EOF5	−3.77	<0.001	500
EOF7	−2.50	<0.001	490
EOF8	−6.08	<0.001	**518**
EOF9	3.38	<0.001	499
EOF10	−3.65	<0.001	501
EOF12	6.26	<0.001	**524**
EOF13	−4.81	<0.001	**510**
EOF15	2.84	<0.001	493
EOF20	2.60	<0.001	495

selected as predictors by the GLM model) are shown in Figure 7. The first EOF, which explains 13% of variability in the SLPa field, appears to be a wave number-1 pattern with only one trough (blue) and one crest (red) illustrating a large-scale pattern. The trough and crest represent anomalous low and high SLP, respectively. For the January 1995 flood event, (1) a strong anomalous low pressure was active with high amplitude when heavy precipitation fell in late January 1995 in France heavy-precipitation area throughout the period; (2) as the end of the heavy rainy period was approached (the 24th Jan), the energy of the low pressure system began to dissipate as illustrated in the Figure 5 covering the SLPa field from the 24th to the 28th, January. The EOF1 time series in January 1995 (Figure 6) shows that the contribution of the EOF1 to anomalous low pressure intensified from the beginning of the rainy period, and changes to a high pressure marking the end of the rainfall event.

[46] The second EOF, which contributes 9.75% of the variability, has two crests (strong positive SLPa) in France and the North Pacific, with a longitudinally elongated low SLPa trough across the entire midlatitude Eurasian continent and a relatively mild low pressure sitting between the two crests. The EOF2 time series (Figure 6) shows an abrupt drop to negative coefficients when the EOF1 began to climb 3 days before the rainy days (on the 13th), indicating synergetic effects in intensifying low pressure over the study region. The negative coefficient of EOF2 starting from the 13th, lasting until after the end of the month, suggests that a persistent low pressure corresponding to this mode was present over Western France.

[47] EOF3 is positively correlated with daily rainfall, but in the GLM its contribution relative to other predictors is relatively small. Its spatial pattern (Figure 7) shows an adjacent trough and crest feature, with the low SLPa centered southwest of France and the high SLPa northeast of France. The EOF3 time series (Figure 6) shows that a positive phase was active from the 13th of January to the 21st, when an abrupt change to negative occurred. This suggested a low pressure was developed southwest of France, 4 days before the onset of heavy persistent rainfall and persistent through the event.

[48] The fourth and fifth EOFs appear to have comparable contributions with positive and negative correlations respectively with daily rainfall. Both have an approximately wave number 3 pattern. However, their temporal expression in January 1995 is quite different. EOF4 persists in a negative state during the event, while EOF5 persists in a positive state for much of the period prior to and during the event with a transition to a negative state marking the end of the event, consistent with its negative correlation with the daily precipitation.

[49] EOF8 has a wave number between 3 and 4. It is negatively correlated with daily precipitation. During the 1995 event it is in a positive mode from Jan. 22–24, and close to zero otherwise. These are the dates (Figures 2 and 4), when the precipitation released in the area is actually small, in the overall 2 week period of rainfall.

[50] EOFs 12 and 13 have wave numbers close to 5 or 6 and explain roughly equal variance in the SVD analysis, suggesting that they may be in quadrature as a transient space-time oscillation. Their correlations with daily precipitation are positive and negative, respectively. In the 1995 expression of these patterns (Figure 6), we notice that they exhibit much higher frequency fluctuations, with an approximate period of 5 days. This is consistent with the time scale expected for transient eddies that are often coupled to the larger scale stationary wave patterns represented for instance by EOFs 1 and 2. Their variations are approximately in quadrature, and accounting for their sign, they typically lead the precipitation in the region by about a day.

[51] The sum of the more persistent high amplitude, low wave number (i.e., large scale) patterns represented by EOFs 1 and 2 and the leading higher wave number transient patterns that reflect the two blocking centers and trapped low are found to be the mechanism associated with the 1995 flood event. The TMEs follow a meridional flow, as is typical, and are then transported into the convergence zone over Western France defined by this persistent pattern. The results found here are consistent with the standard theory on transient eddy-mean flow stationary wave interactions, and with the mechanisms articulated for TME emergence. The attribution of their contribution to a specific extreme

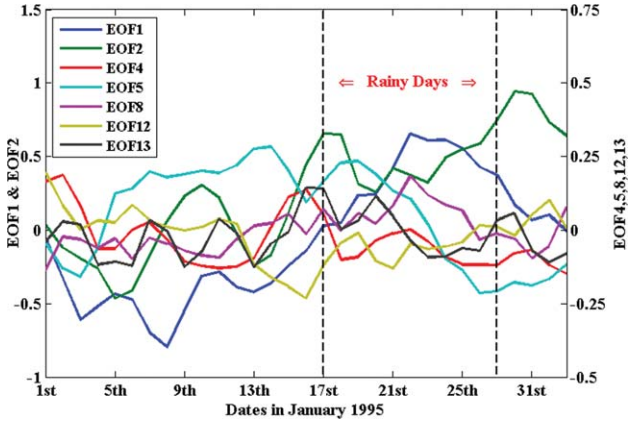

Figure 6. Time series of contribution of selected EOFs' (EOF1, EOF2, EOF4, EOF5, EOF8, EOF12, and EOF13) as measured by the product of their GLM coefficients (β) and the EOF time series for January 1995. Note that EOFs 1 and 2 are plotted using the y-axis scale on the left, since they dominate and the others are plotted using the y-axis scale on the right so that their time series amplitude can be discerned.

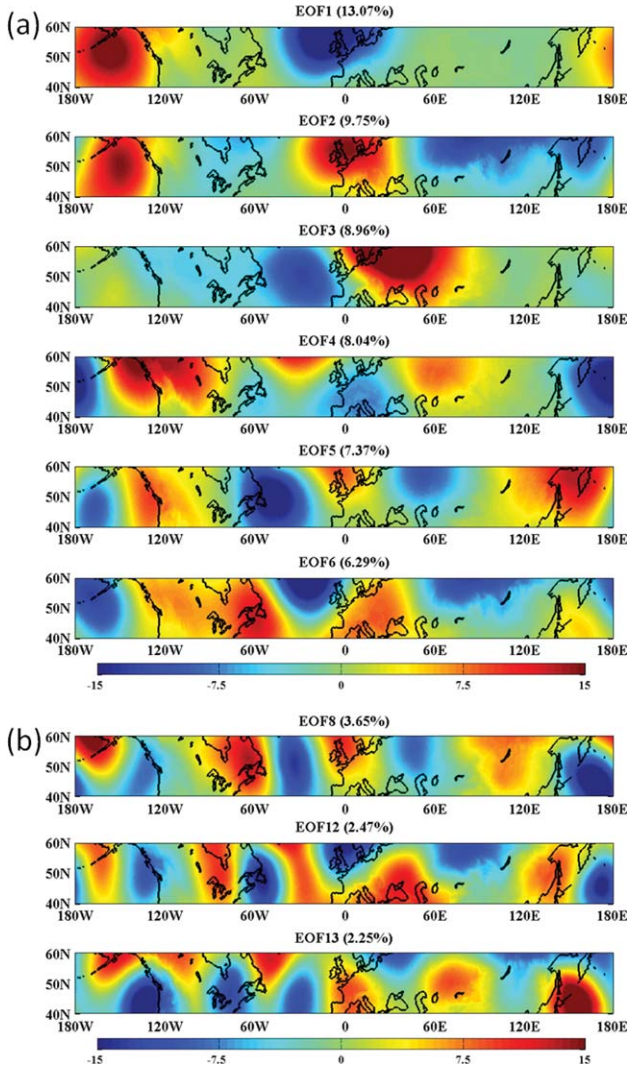

Figure 7. (a) First six EOFs representing the prominent spatial patterns of daily SLPa of Januaries from 1979 to 2011; (b) EOFs 8, 12, 13 that were also selected by the GLM with significant contributions in the model. The color bar indicates the amplitudes of the high pressures (crests of the waves) and low pressures (troughs of the waves).

rainfall event is remarkable, as shown by the day-by-day predictions from the GLM that uses only these patterns and no direct information about the atmospheric moisture content as predictors. This is shown in Figure 8, through the conditional mean and the 95% prediction intervals which appear to provide excellent coverage of the extreme 1995 area-averaged rainfall. In this out of sample prediction, 53% of the total variance of the January rainfall in 1995 is explained by the conditional mean from the GLM. We remind the reader that this was not intended to be a daily rainfall forecast model. Rather, the interest was in establishing how much of the daily rainfall variance could be attributed to the atmospheric circulation pattern, to establish the importance of understanding their role in future projections of extreme rainfall as opposed to purely an increase in the atmospheric moisture content due to warming.

5.3. The NAO Index, Extreme Precipitation, and the SLPa

[52] The winter NAO is often cited as a determinant of seasonal precipitation and temperature in N. Europe. Consequently, we explored its potential role in determining extreme precipitation as well as the associated atmospheric circulation patterns in the study area. The direct correlations of daily area averaged rainfall in the region and the daily NAO were significant at the 5% level but low ($\sim$ 0.1) for 0 to 3 days preceding rainfall. The NAO correlations were statistically significant with the SLPa EOFs 1, 3, 4, 5, 6, 7, 9, 10, and 14. The highest correlations ($\sim$0.3–0.46) are with EOFs 4–6 and 10. Since the NAO is derived through a SVD analysis of the North Atlantic SLP field, these associations are expected. The finding remains that it is useful to explore the role of the larger-scale atmospheric circulation field on regional midlatitude extreme precipitation directly, rather than using only a regional circulation index.

6. Summary and Conclusions

[53] A mechanistic understanding of extreme floods requires an understanding and characterization of their causal factors. Traditionally, hydrologists focused on landscape scale hydrologic processes, viewing rainfall as a known or stochastic exogenous forcing. The role of atmospheric processes has received much more attention in recent years, as hydrometeorology and hydroclimatology have evolved as fields. *Lavers et al*. [2013] showed that under future climate projections, North Atlantic ARs are projected to become stronger and more numerous in the future scenarios of multiple simulations from five state-of-the-art global climate models (GCMs) in the fifth Climate Model Intercomparison Project. The synoptic structure of atmospheric fields and their connection to larger scale features is being explored in this context. A specific genre of interest in this regard is the association of TMEs (or ARs) with major floods in the midlatitudes. These are large-scale climate features whose recurrence is of considerable interest for future flood potential, especially considering

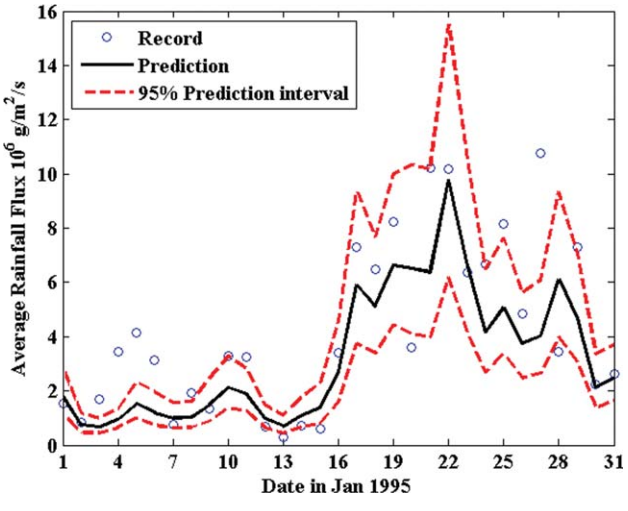

Figure 8. Predicted area average rainfall in January 1995 using concurrent SLPa EOFs by fitted GLM using dataset excluding 1995.

changes in atmospheric circulation that may emerge as part of natural modes of climate variability or anthropogenic forcing. With this context in mind, we explored four questions associated with a large-scale, persistent flooding event that took place over Northern France in January 1995.

[54] As in *Nakamura et al*. [2012] analysis of the Ohio River Basin, we find that the tropical Atlantic Ocean provides the moisture source for the extreme rainfall leading to floods, and that large-scale atmospheric circulation pattern anomalies govern the associated dynamics of the associated TMEs and their convergence and moisture release in the flooded area. A significant finding is that the largest contribution comes from a hemispheric stationary wave pattern rather than from local circulation patterns and indices, though interactions between the different scales are clearly important. These patterns established from data excluding the extreme January 1995 period were able to explain 53% of the variation in daily rainfall, and provide a good coverage for the extreme daily rainfall events for January 1995. This observation reinforces the notion that one needs to assess potential changes in the atmospheric circulation as well as potential changes in the atmospheric moisture content, and in tropical convection to determine changes in future extreme rainfall intensity and duration. At the same time, the simple analyses presented here point to the promise for diagnosing extreme precipitation patterns from future integrations of Ocean-Atmosphere General Circulation Models (GCMs).

[55] It is well known that historical precipitation simulated from GCMs tends to have large biases and hydrologists [e.g., *Johnson and Sharma*, 2012] often apply bias correction methods to this output, without an effort to understand or diagnose the source of the bias. The findings of this paper suggest that for midlatitude extreme precipitation associated with TME, it is important to understand the large-scale mean flow and the eddies coupled to it. *Lorenz* [1984, 1990] presents a low order dynamical model for the midlatitude atmospheric circulation as described by the interactions between the mean flow and the transient eddies that is forced by the equator to pole temperature gradient (EPG) and the land ocean temperature contrast. The model solutions demonstrate multiple potential equilibrium solutions, chaos, and intransitivity. An interesting aspect of the model solutions is that persistent blocking regimes of the sort that correspond to the extreme flood event discussed here are generated. Subsequently, [*Rind*, 1998; *Jain et al*., 1999; *Karamperidou et al*., 2012] EPG and OLC were used as diagnostic indicators of how climate change may manifest in the circulation. *Jain et al*. [1999] showed that the GCM simulations of the 20th century climate had significant biases in both EPG and OLC relative to the estimates from observations. *Karamperidou et al*. [2012] showed that the newer generation of GCMs was still biased for EPG and OLC, that there were resulting biases in the location and strength of the midlatitude circulation, and that models with smaller biases in EPG and OLC had correspondingly smaller biases in the midlatitude jet variables and in the mean precipitation field. The present paper reinforces these observations empirically by establishing that for extreme precipitation, one need to get the large-scale mean flow and its interactions with eddies right, so that the steering and convergence of tropical moisture is properly modeled. It would be good to check whether a particular climate model does reproduce these features in a historical simulation, before considering its use for future extreme precipitation simulations.

[56] A number of areas need to be explored and modeled to move to a formal predictive strategy. Specifically, one could explore whether intraseasonal oscillations, such as the Madden Julian Oscillation, with a 20–40 day period, that is, associated with modes of tropical convection [*Kiladis and Weickmann*, 1992; *Maloney and Hartmann*, 2000, 2001; *Barrett and Leslie*, 2009], and slowly evolving large-scale extratropical circulation modes interact to determine the circulation patterns that lead to both the moisture transport and the persistent regional atmospheric convergence that appears to be associated with these extreme events. Further, the ability to use the SLPa EOFs to offer reasonable linear prediction of the extreme daily rainfall offers the opportunity to explore predictive modeling with nonlinear and delay terms with SLPa, lagged precipitation, and other state variables in a search for a low dimensional analog for the large-scale climate dynamics that may drive seasonal rainfall extremes. Such a model would help both conceptual understanding of these phenomena for hydroclimate researchers and provide practical advances in short term prediction or the projection of long term climate scenarios for a region. Both are key building blocks for an understanding and analysis of nonstationary flood risk dynamics.

[57] **Acknowledgments.** This work was supported by National Research Foundation of Korea Grant funded by the Korean Government (NRF-2010-220-D00083). This work was part of the titled "Climate Informed Global Flood Risk Assessment" project supported by Chartis Global Services. The authors also sincerely appreciate the constructive comments from the associate editor and anonymous reviewers.

References

Allan, R. P., and B. J. Soden (2008), Atmospheric warming and the amplification of precipitation extremes, *Science*, *321*, 1481–1484, doi:10.1126/science.1160787.

Bao, J.-W., S. A. Michelson, P. J. Neiman, F. M. Ralph, and J. M. Wilczak (2006), Interpretation of enhanced integrated water vapor bands associated with extratropical cyclones: their formation and connection to tropical moisture, *Month. Weather Rev.*, *134*, 1063–1080, doi:10.1175/MWR3123.1. [online] Available at: http://dx.doi.org/10.1175/MWR3123.1.

Barrett, B. S., and L. M. Leslie (2009), Links between tropical cyclone activity and Madden–Julian oscillation phase in the North Atlantic and Northeast Pacific Basins, *Month. Weather Rev.*, *137*, 727–744, doi:10.1175/2008MWR2602.1.

Bissolli, P., K. Friedrich, J. Rapp, and M. Ziese (2011), Flooding in eastern central Europe in May 2010–reasons, evolution and climatological assessment, *Weather*, *66*, 147–153, doi:10.1002/wea.759.

Bretherton, C. S., C. Smith, and J. M. Wallace (1992), An intercomparison of methods for finding coupled patterns in climate data, *J. Climate*, *5*, 541–560, doi:10.1175/1520-0442(1992)005<0541:AIOMFF>2.0.CO;2.

Cherry, S. (1997), Some comments on singular value decomposition analysis, *J. Climate*, *10*, 1759–1761, doi:10.1175/1520-0442(1997)010<1759:SCOSVD>2.0.CO;2.

Everitt, S. B., and G. Dunn (2001), Applied Multivariate Data Analysis, Arnold, London.

Gnanadesikan, R. (1997), *Methods for Statistical Data Analysis of Multivariate Observations*, John Wiley & Sons, N. Y.

Held, I. M., and B. J. Soden (2006), Robust responses of the hydrological cycle to global warming, *J. Climate*, *19*, 5686–5699, doi:10.1175/JCLI3990.1.

Jain, S., and U. Lall (2000), Magnitude and timing of annual maximum floods: Trends and large-scale climatic associations for the Blacksmith Fork River, Utah, *Water Resour. Res.*, *36*, 3641–3651, doi:10.1029/2000WR900183.

Jain, S., and U. Lall (2001), Floods in a changing climate: Does the past represent the future?, *Water Resour. Res.*, *37*, 3193, doi:10.1029/2001WR000495.

Jain, S., U. Lall, and M. E. Mann (1999), Seasonality and interannual variations of Northern Hemisphere temperature: Equator-to-pole gradient and ocean–land contrast, *J. Climate*, *12*, 1086–1100, doi:10.1175/1520-0442(1999)012<1086:SAIVON>2.0.CO;2.

Johnson, F., and A. Sharma (2012), A nesting model for bias correction of variability at multiple time scales in general circulation model precipitation simulations, *Water Resour. Res.*, *48*, W01504, doi:10.1029/2011WR010464.

Karamperidou, C., F. Cioffi, and U. Lall (2012), Surface temperature gradients as diagnostic indicators of midlatitude circulation dynamics, *J. Climate*, *25*, 4154–4171, doi:10.1175/JCLI-D-11-00067.1.

Katz, R. W. (2010), Statistics of extremes in climate change, *Climatic Change*, *100*, 71–76, doi:10.1007/s10584-010-9834-5.

Kharin, V. V., and F. W. Zwiers (2000), Changes in the extremes in an ensemble of transient climate simulations with a coupled atmosphere–ocean GCM, *J. Climate*, *13*, 3760–3788, doi:10.1175/1520-0442(2000)013<3760:CITEIA>2.0.CO;2.

Kharin, V. V., and F. W. Zwiers (2005), Estimating extremes in transient climate change simulations, *J. Climate*, *18*, 1156–1173, doi:10.1175/JCLI3320.1.

Kiladis, G. N., and K. M. Weickmann (1992), Circulation anomalies associated with tropical convection during Northern Winter, *Mon. Weather Rev.*, *120*, 1900–1923, doi:10.1175/1520-0493(1992)120<1900:CAAWTC>2.0.CO;2.

Knippertz, P., and H. Wernli (2010), A Lagrangian climatology of tropical moisture exports to the northern hemispheric extratropics, *J. Climate*, *23*, 987–1003, doi:10.1175/2009JCLI3333.1.

Knippertz, P., H. Wernli, and G. Gläser (2012), A global climatology of tropical moisture exports, *J. Climate*, *26*, 3031–3045, doi:10.1175/JCLI-D-12-00401.1.

Lanzante, J. R. (1984), A rotated Eigenanalysis of the correlation between 700 mb heights and sea surface temperatures in the Pacific and Atlantic', *Month. Weather Rev.*, *112*, 2270–2280, doi:10.1175/1520-0493(1984)112<2270:AREOTC>2.0.CO;2.

Lavers, D. A., R. P. Allan, E. F. Wood, G. Villarini, D. J. Brayshaw, and A. J. Wade (2011a), Winter floods in Britain are connected to atmospheric rivers, *Geophys. Res. Lett.*, *38*, L23803, doi:10.1029/2011GL049783.

Lavers, D. A., R. P. Allan, E. F. Wood, G. Villarini, D. J. Brayshaw, and A. J. Wade (2011b), Winter floods in Britain are connected to atmospheric rivers, *Geophys. Res. Lett.*, *38*, L23803, doi:10.1029/2011GL049783.

Lavers, D. A., R. P. Allan, G. Villarini, B. Lloyd-Hughes, D. J. Brayshaw, and A. J. Wade (2013), Future changes in atmospheric rivers and their implications for winter flooding in Britain, *Environ. Res. Lett.*, *8*, 034010, doi:10.1088/1748-9326/8/3/034010.

Lima, C. H. R., and U. Lall (2010), Spatial scaling in a changing climate: A hierarchical bayesian model for non-stationary multi-site annual maximum and monthly streamflow, *J. Hydrol.*, *383*, 307–318, doi:10.1016/j.jhydrol.2009.12.045.

Lorenz, E. N. (1956), Empirical orthogonal functions and statistical weather prediction, *Tech. Rep. Stat. Forecast Project Rep. 1 Dept. Meteorol. 1*, 52.

Lorenz, E. N. (1984), Irregularity: A fundamental property of the atmosphere, *Tellus A*, *36A*, 98–110, doi:10.1111/j.1600-0870.1984.tb00230.x.

Lorenz, E. N. (1990), Can chaos and intransitivity lead to interannual variability?, *Tellus A*, *42*, 378–389, doi:10.1034/j.1600-0870.1990.t01-2-00005.x.

Maloney, E. D., and D. L. Hartmann (2000), Modulation of Hurricane Activity in the Gulf of Mexico by the Madden-Julian Oscillation, *Science*, *287*, 2002–2004, doi:10.1126/science.287.5460.2002.

Maloney, E. D., and D. L. Hartmann (2001), The Madden–Julian oscillation, barotropic dynamics, and North Pacific Tropical cyclone formation. Part I: Observations, *J. Atmos. Sci.*, *58*, 2545–2558, doi:10.1175/1520-0469(2001)058<2545:TMJOBD>2.0.CO;2.

Marsh, T. J., (2004), The January 2003 flood on the Thames, *Weather*, *59*, 59–62, doi:10.1256/wea.212.03.

Marsh, T. J., and M. Dale (2002), The UK Floods of 2000–2001: A Hydrometeorological Appraisal, *Water Environ. J.*, *16*, 180–188, doi:10.1111/j.1747-6593.2002.tb00392.x.

Massei, N., and M. Fournier (2012), Assessing the expression of large-scale climatic fluctuations in the hydrological variability of daily Seine river flow (France) between 1950 and 2008 using Hilbert–Huang Transform, *J. Hydrol.*, *448–449*, 119–128, doi:10.1016/j.jhydrol.2012.04.052.

McCullagh, P., and J. A. Nelder (1989), *Generalized Linear Models*, 2nd ed., Chapman & Hall, London.

Mcleod, A., and C. Xu (2010), bestglm: Best Subset GLM, Prostate The, *1–39*. [Available at http://cran.r-project.org/web/packages/bestglm/vignettes/bestglm.pdf.]

Muller, C. J., P. A. O'Gorman, and L. E. Back (2011), Intensification of precipitation extremes with warming in a cloud-resolving model, *J. Climate*, *24*, 2784–2800, doi:10.1175/2011JCLI3876.1.

Nakamura, J., U. Lall, Y. Kushnir, A. W. Robertson, and R. Seager (2012), Dynamical structure of extreme floods in the U.S. Midwest and the UK, *J. Hydrometeorol.*, doi:10.1175/JHM-D-12-059.1.

Olsen, J. R., J. R. Stedinger, N. C. Matalas, and E. Z. Stakhiv (1999), Climate variability and flood frequency estimation for the upper Mississippi and lower Missouri rivers, *J. Am. Water Resour. Assoc.*, *35*, 1509–1523, doi:10.1111/j.1752-1688.1999.tb04234.x.

Prohaska, J. T. (1976), A technique for analyzing the linear relationships between two meteorological fields, *Month. Weather Rev.*, *104*, 1345–1353, doi:10.1175/1520-0493(1976)104<1345:ATFATL>2.0.CO;2.

Ralph, F. M., and M. D. Dettinger (2011), Storms, floods, and the science of atmospheric rivers, *Eos, Trans. Am. Geophys. Union*, *92*, 265, doi:10.1029/2011EO320001.

Renard, B., M. Lang, and P. Bois (2006), Statistical analysis of extreme events in a non-stationary context via a Bayesian framework: Case study with peak-over-threshold data, *Stochastic Environ. Res. Risk Assess.*, *21*, 97–112, doi:10.1007/s00477-006-0047-4.

Rienecker, M. M., et al. (2011), MERRA: NASA's modern-era retrospective analysis for research and applications, *J. Climate*, *24*, 3624–3648, doi:10.1175/JCLI-D-11-00015.1.

Rind, D. (1998), Latitudinal temperature gradients and climate change, *J. Geophys. Res.*, *103*, 5943, doi:10.1029/97JD03649.

Romps, D. M. (2011), Response of tropical precipitation to global warming, *J. Atmos. Sci.*, *68*, 123–138, doi:10.1175/2010JAS3542.1.

Sánchez, J. (1982), MARDIA, K. V., J. T. KENT, J. M. BIBBY: Multivariate Analysis. Academic Press, London-New York-Toronto-Sydney-San Francisco 1979. xv, 518 pp., *Biom. J.*, *24*, 502, doi:10.1002/bimj.4710240520.

Schubert, S., H. Wang, and M. Suarez (2011), Warm season subseasonal variability and climate extremes in the Northern Hemisphere: The role of stationary rossby waves, *J. Climate*, *24*, 4773–4792, doi:10.1175/JCLI-D-10-05035.1.

Schwarz, G. (1978), Estimating the dimension of a model, *Ann. Stat.*, *6*, 461–464, doi:10.1214/aos/1176344136.

Semenov, V. and L. Bengtsson (2002), Secular trends in daily precipitation characteristics: Greenhouse gas simulation with a coupled AOGCM, *Climate Dyn.*, *19*, 123–140, doi:10.1007/s00382-001-0218-4.

Sirca, S., and M. Horvat (2012), *Computational Methods for Physicists: Compendium for Students*, Springer, Heidelberg, New York.

Trenberth, K. E., A. Dai, R. M. Rasmussen, and D. B. Parsons (2003), The Changing Character of Precipitation, *Bull. Am. Meteor. Soc.*, *84*, 1205–1217, doi:10.1175/BAMS-84-9-1205.

Ulbrich, U., T. Brücher, A. H. Fink, G. C. Leckebusch, A. Krüger, and J. G. Pinto (2003a), The central European floods of August 2002: Part 1 – Rainfall periods and flood development, *Weather*, *58*, 371–377, doi:10.1256/wea.61.03A.

Ulbrich, U., T. Brücher, A. H. Fink, G. C. Leckebusch, A. Krüger, and J. G. Pinto (2003b), The central European floods of August 2002: Part 2 – Synoptic causes and considerations with respect to climatic change, *Weather*, *58*, 434–442, doi:10.1256/wea.61.03B.

Villarini, G., F. Serinaldi, J. A. Smith, and W. F. Krajewski (2009), On the stationarity of annual flood peaks in the continental United States during the 20th century, *Water Resour. Res.*, *45*, 1–17, doi:10.1029/2008WR007645.

Voss, R., W. May, and E. Roeckner (2002), Enhanced resolution modelling study on anthropogenic climate change: changes in extremes of the hydrological cycle, *Int. J. Climatol.*, *22*, 755–777, doi:10.1002/joc.757.

Webster, P. J., V. E. Toma, and H. M. Kim (2011), Were the 2010 Pakistan floods predictable?, *Geophys. Res. Lett.*, *38*, 1–5, doi:10.1029/2010GL046346.

Wehner, M. F. (2004), Predicted twenty-first-century changes in seasonal extreme precipitation events in the parallel climate model, *J. Climate*, *17*, 4281–4290, doi:10.1175/JCLI3197.1.

Wilby, R. L., and T. M. L. Wigley (2002), Future changes in the distribution of daily precipitation totals across North America., *Geophys. Res. Lett.*, *29*, 1999–2002, doi: 10.1029/2001GL013048.

Zhu, Y., and R. E. Newell (1998), A proposed algorithm for moisture fluxes from atmospheric rivers, *Month. Weather Rev.*, *126*, 725–735, doi:10.1175/1520-0493(1998)126<0725:APAFMF>2.0.CO;2.

Zong, Y., and X. Chen (2000), The 1998 Flood on the Yangtze, China, *Nat. Hazards*, *22*, 165–184, doi:10.1023/A:1008119805106.